Spin-one bilinear-biquadratic model on a star lattice

Hyun-Yong Lee[*] and Naoki Kawashima[†]

Institute for Solid State Physics, University of Tokyo, Kashiwa, Chiba 277-8581, Japan

We study the ground-state phase diagram of the $S = 1$ bilinear-biquadratic model (BLBQ) on the star lattice with the state-of-art tensor network algorithms. The system has four phases: the ferromagnetic, antiferromagnetic, ferroquadrupolar, and spin-liquid phases. The phases and their phase boundaries are determined by examining various local observables, correlation functions, and transfer matrices exhaustively. The spin-liquid phase, which is the first quantum disordered phase found in the two-dimensional BLBQ model, is gapped and devoid of any conventional long-range order. It is also characterized by fixed-parity virtual bonds in the tensor network formalism, analogous to the Haldane phase, while the parity varies depending on the location of the bond.

I. INTRODUCTION

After the discovery of the high-temperature superconductors [1], their parent compounds are conjectured to be in a spin-liquid (SL) phase which becomes superconducting when charge carriers are doped [2]. Such SLs are expected to possess a kind of quantum order [3–5], e.g., Z_2 topological order in Z_2-SLs [3,4], or support fractionalized edge excitations protected by some symmetries [6], e.g., Haldane phase [7–10]. Quantum effects or fluctuations are believed to become stronger as the spin and spatial dimension decrease. The geometric frustration also plays an important role [11]. Consequently, with the successful realizations of the kagome lattice in volborthite [12], herbertsmithite [13], and kapellasite [14] and the triangular lattice in κ-BEDT(CN)$_3$ [15], the frustrated $S = \frac{1}{2}$ systems have been extensively studied to find stable SL states. However, the recent discoveries of SLs in the pnictide family of superconductors [16,17] and an unconventional quantum disordered state in Ba$_3$NiSb$_2$O$_9$ [18] triggered a burst of investigations on $S = 1$ quantum magnets on square [19–29], honeycomb [30,31], kagome [32], and triangular [33,34] lattices, respectively. Theoretically, such lattices can be decorated to be so-called star lattices of which the geometry is distinct from the ones of lattices listed above. Generally, such decoration may cause nontrivial results on the state with strong fluctuations. One may, therefore, seek novel spin-liquid states in such lattices [35–37]. In fact, previous studies on the star lattice spin-1/2 models found an exact chiral SL with non-Abelian anyonic excitations [38–40], various valence-bond-solid (VBS) ground states (GS) [41,42], and topological order in several SL phases [43,44].

Theoretical and computational studies on the strongly correlated systems are entering a new phase under the remarkable development in the tensor network (TN) algorithms. We refer the readers to Ref. [45] for an exhaustive list of relevant literature. The TN method does not suffer from the sign problem for the frustrated models and also allows us to reach the thermodynamic limit efficiently by employing the framework of renormalization group [46,47]. Advantage of the tensor network representation is not only technical but also conceptual; information on the GS entanglement is directly accessible by looking at the geometry of TN and gauge symmetry of local tensors [45,48]. A well-known example is the Haldane phase (and its generalization to higher dimensions) that can be characterized very clearly by the fixed parity of the virtual bonds in their tensor network representations [10]. In this sense, the TN method is ideal to investigate SL, and a lot of approaches have been already proposed in recent years [see Ref. [49] and references therein]. In the present article, we employ TN algorithms to explore the $S = 1$ BLBQ model on the star lattice [Fig. 1(a)].

II. MODEL

Let us begin with defining the BLBQ model:

$$H = \sum_{\langle i,j \rangle} \left[\left(\cos\phi - \frac{\sin\phi}{2} \right) \boldsymbol{S}_i \cdot \boldsymbol{S}_j + \frac{\sin\phi}{2} \boldsymbol{Q}_i \cdot \boldsymbol{Q}_j \right], \quad (1)$$

where $\langle i,j \rangle$ denotes the nearest-neighbor sites, $\boldsymbol{S}_i$ is the spin-one operator, and $\boldsymbol{Q}_i$ is the quadrupolar (QD) operator with five components: $(S_i^x)^2 - (S_i^y)^2$, $\sqrt{3}(S_i^z)^2 - 2/\sqrt{3}$, $S_i^x S_i^y + S_i^y S_i^x$, $S_i^y S_i^z + S_i^z S_i^y$, and $S_i^z S_i^x + S_i^x S_i^z$. The quadrupole moment $Q \equiv N_s^{-1} \sum_i^{N_s} \sqrt{\langle \boldsymbol{Q}_i \rangle^2}$, where N_s is the total number of lattice sites, is a fundamental order parameter identifying the phases in the BLBQ model on various lattices [19,20,31,33,50–52]. Note that at some special values of ϕ the system possesses the symmetry higher than the obvious SU(2) symmetry. At $\phi = -3\pi/4, \pi/4$, the Hamiltonian is invariant under simultaneous SU(3) rotations at all lattice points.

III. METHOD

To carve out the GS phase diagram of the model in Eq. (1), we optimize the inifinite projected entangled pair states (iPEPS) with a rank-four site tensor $T^{s_i}_{x_i y_i z_i}$ and singular value matrices $\lambda_{\alpha_i \alpha_i'}$ [53,54]: $|\psi\rangle =$

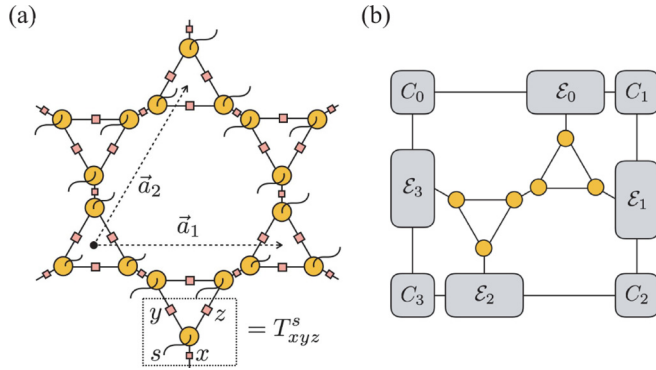[*]hyunyong.rhee@gmail.com

[†]kawashima@issp.u-tokyo.ac.jp

FIG. 1. Schematic figures of (a) iPEPS (yellow circle, site tensor; red square, singular value matrix) on the star lattice ($\vec{a}_{1,2}$, lattice vector) and (b) environment tensors $\{C_i, \mathcal{E}_i\}$ and double layered tensors in the unit cell. Here, T^s_{xyz} in the dashed box denotes the site tensor (see the main text for details).

$\sum_{\{\alpha_i\}} \mathrm{Tr} \prod_i T^{s_i}_{x_i y_i z_i} \lambda^{1/2}_{x_i x_i'} \lambda^{1/2}_{y_i y_i'} \lambda^{1/2}_{z_i z_i'} |s_i\rangle$, where Tr represents the trace over the virtual indices (x_i, y_i, z_i) and s_i is the local quantum number. Its graphical representation is shown in Fig. 1(a). For convenience later, we define the bond connecting two triangle plaquettes as x bond and two bonds forming a triangle plaquette as y and z bonds in the clockwise direction as depicted in Fig. 1(a). By applying iteratively the imaginary-time evolution operator $[\exp(-\tau H_{ij})]$ on every bond, one can optimize $T^{s_i}_{x_i y_i z_i}$ with respect to the energy density. The simple update (SU) is a popular method to renew the tensors at every imaginary-time step [54]. Recently, the importance of preserving symmetries in optimization has been noticed with a development of so-called symmetric simple update (SSU), which allows us to keep symmetries throughout the imaginary-time evolution [49]. In this paper, either SU or SSU is adopted depending on the initial and target states. To be more precise, we examine three kinds of ansatz: SU(2) symmetric, time-reversal (TR) symmetric, and nonconstraint ansatz. We try several initial conditions for each type of ansataz, e.g., the ferromagnetic (FM), 120° coplanar antiferromagnetic (AFM) product states and random states for the nonconstraint ansatz. In order to contract iPEPS without symmetry breaking, we apply the basic idea of SSU to the corner transfer matrix renormalization group (CTMRG) method [37,55–59]. Then, we measure the physical quantities, such as the local order parameters and correlation functions, using the environment tensors obtained by CTMRG. The parallel C++ library *mptensor* [60] is utilized to perform all TN algorithms in the present work.

IV. IDENTIFICATION OF EACH PHASE

GS phase diagram is presented in Fig. 2, in which four phases are identified: FM, ferroquadrupolar (FQ), AFM, and SL. We have determined those phases by analyzing the energy density, local order parameters, and the connected correlation functions for the optimized ansatz on a variety of unit-cell structures [61] with trial initial states. The bond dimension D for the virtual legs is varied from 1 to 12, and the GSs are adopted at each ϕ by the lowest energy density shown
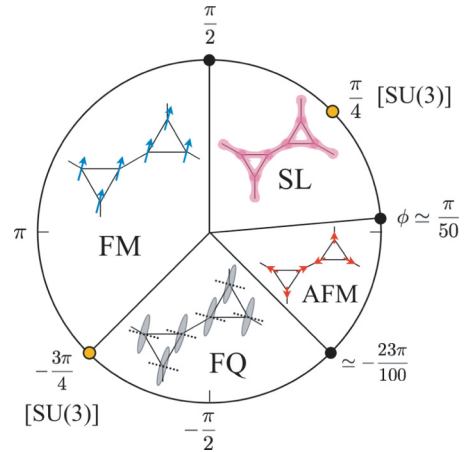

FIG. 2. Phase diagram of the BLBQ model on the star lattice [Eq. (1)] as a function of the mixing angle ϕ. Here, FM, FQ, AFM, and SL represent ferromagnetic, ferroqudrupolar, 120° coplanar antiferromagnetic, and spin-liquid phases, respectively. The model has the SU(3) symmetry at $\phi = -0.75\pi, 0.25\pi$ which are denoted by yellow circles.

in Fig. 3(a). A cutoff dimension χ for CTMRG is chosen to be $\chi = 2D^2$. Here, we identify and discuss the properties of each phase, and then the nature of phase boundaries will be discussed afterward.

Regardless of the spatial dimension or the lattice geometry, the BLBQ model exhibits FM phase in $0.5\pi < \phi < 1.25\pi$ [32,33,51,54,62] as we also found. In this phase, the imaginary time evolution with SU leads the tensors to a trivial tensor with $D = 1$, i.e., a product state. Throughout this phase, the
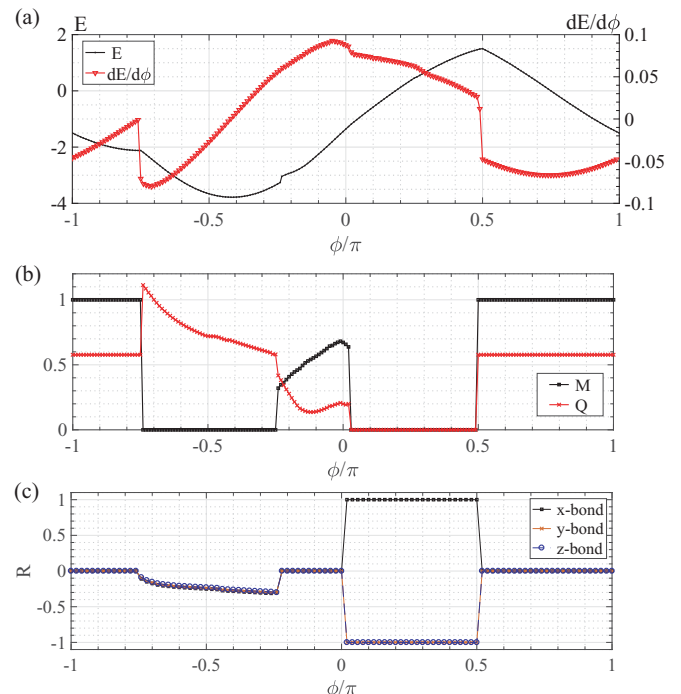

FIG. 3. Plots of the (a) energy density, (b) magnetization and quadrupole moments of GS wave function, and (c) the quantity R defined in Eq. (2) as a function of ϕ, respectively.

magnetization $M \equiv N_s^{-1} \sum_i^{N_s} \sqrt{\langle S_i \rangle^2}$ is always 1, and $Q = 1/\sqrt{3}$ indicating fully aligned spins.

The FQ phase occurs right next to FM phase at $\phi = -0.75\pi$ and disappears at $\phi \simeq -0.23\pi$ where the GS enters into AFM phase. Since BQ interaction with negative sign favors parallel alignment of the quadrupole moments, the FQ state becomes stable immediately after BQ wins BL exchange ($\phi > -0.75\pi$). The FQ order parameter gradually decreases from the largest value $Q(\phi = -0.75\pi) = 2/\sqrt{3}$ as ϕ approaches to -0.23π, while the magnetization is always zero up to the machine precision. The TR-symmetric initial state with SSU flows into the lowest energy state resulting in $M = 0$ all through this phase. We find that $\lambda_{\alpha_i \alpha_i'}$ are rotationally symmetric (i.e., $\lambda_{x_i x_i'} = \lambda_{y_i y_i'} = \lambda_{z_i z_i'}$) and carry nondegenerate and doubly degenerate values. It denotes that the site tensor accommodates the Kramers singlets and doublets on the virtual legs to form a TR-symmetric tensor.

As ϕ passes through -0.23π, the magnetization jumps from zero [Fig. 3(b)], and spins form the 120° coplanar configuration. The FQ order parameter remains finite due to the finite magnetization. The magnetization reaches the maximum at $\phi = 0$ where BQ exchange is turned off, and this is similar to the triangular and honeycomb models [31,33]. The AFM phase, which is obtained by SU with the 120° coplanar initial configuration, seems to extend to $\phi \simeq 0.02\pi$. However, it is not exactly determined as the iPEPS optimization does not converge well and thus shows some fluctuations in the energy density and order parameters over $0 < \phi \lesssim 0.02\pi$. Nevertheless, AFM state gives still the lowest energy of all.

In $0.02\pi \lesssim \phi < 0.5\pi$, the SU(2)-symmetric SSU on (1×1) unit cell provides the best ansatz, and therefore the GS is SL throughout this region. By virtue of SSU, we find that only the integer spins are accommodated on the x bond while only the half-integer spins on the y and z bonds. In order to show this interesting feature, we define a quantity

$$R \equiv \frac{\sum_i (d_i - 1)(-1)^{d_i - 1} \lambda_i}{\sum_i \lambda_i}, \qquad (2)$$

where d_i is the degeneracy of the ith singular value λ_i. The R at each bond is presented in Fig. 3(c). Because of the lack of any symmetry, the λ_i does not degenerate, and therefore R is zero throughout the FM and AFM phases. It is finite and changes continuously in the FQ phase because of the double degeneracy of some of the singular values guaranteed by TR symmetry. In the SL phase, the R becomes integer either $+1$ or -1 depending on the bond, which shows that each bond accommodates either only even- or odd-parity multiplets. This is analogous to the Haldane phase, where the virtual bonds carry only the odd-parity multiplets [10].

The positive BQ exchange favors a perpendicular orientation of neighboring quadrupole moments. It induces the antiferroquadrupolar phases on the triangular [33] and kagome [32] lattices, on which spins on a triangle plaquette are shared by neighboring plaquettes. Instead, on the star lattice, spins are not shared but entangled with others on neighboring plaquttes. As a result, it may give rise to configurational fluctuations of quadrupole moments and subsequently the recovery of symmetry.
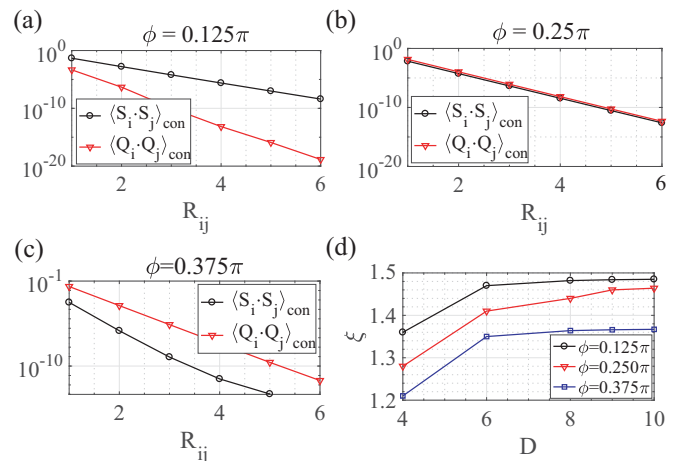

FIG. 4. Spin-spin and quadrupole-quadrupole correlations at (a) $\phi = 0.125$ and (b) $\phi = 0.375\pi$, respectively. Here, R_{ij} is the distance between ith and jth sites in units of $|\vec{a}_1|$ defined in Fig. 1.

In order to explore the physical property of the SL phase, we evaluate the connected spin $C_{ij}^S \equiv \langle S_i \cdot S_j \rangle_{\mathrm{con}}$ and quadrupole $C_{ij}^Q \equiv \langle Q_i \cdot Q_j \rangle_{\mathrm{con}}$ correlators as a function of distance between ith and jth sites, which are shown in Figs. 4(a)–4(c). As one can see, both correlators decay exponentially in the entire SL phase, and especially $C_{ij}^Q = \frac{5}{3} C_{ij}^S$ at $\phi = 0.25\pi$ [Fig. 4(b)], where the SU(3) symmetry emerges. In addition, the dimer and chirality correlators are found to be suppressed exponentially as well. Therefore, we may conclude that there is no long-range order in this phase.

Regarding a quantum liquid phase, the fact of existence or nonexistence of the gap is one of the most important questions. The exponential decaying of correlators in Fig. 4 intimates the gapped nature of the SL phase. In order to confirm this quantitatively, we propose a method for constructing the transfer matrix (X):

$$X_{(\alpha, \alpha'; \beta, \beta')} = \quad (3)$$

where $\mathcal{E}_0$ and $\mathcal{E}_2$ are the edge tensors depicted in Fig. 1(b). Generally, the transfer matrix X is supposed to contain information on the long-range properties of the iPEPS ansatz such as the correlation length [63]: $\xi^{-1} = \log(\lambda_0 / \lambda_1)$, where $\lambda_{0\,(1)}$ is the largest (second largest) eigenvalue of X. The advantage of this method of obtaining ξ over the one based on the two-point correlator of certain quantities is that we do not have to know the quantity that shows the slowest decay. Figure 4(d) shows the extracted ξ at $\phi = 0.125\pi, 0.25\pi, 0.375\pi$ which converge to finite values as D increases and thus clarify the existence of gap in the SL phase. Another transfer matrix made of $\mathcal{E}_1$ and $\mathcal{E}_3$ gives the same correlation length due to the rotational symmetry.

V. PHASE BOUNDARIES

Both the boundaries of the FM phase can be fixed exactly: $\phi = -0.75\pi$ and 0.5π. The boundary to the FQ phase, $\phi = -0.75\pi$, can be fixed as the point at which the system possesses
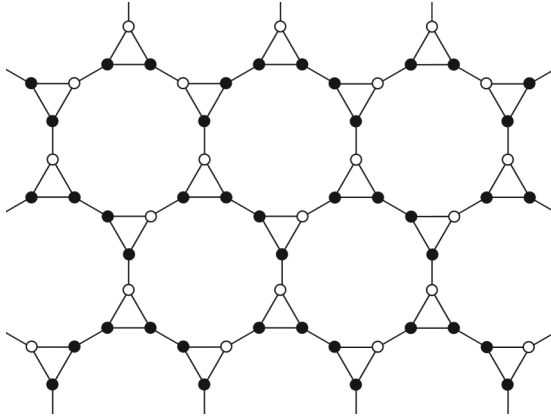
FIG. 5. An exemplary ground-state configuration at the pure biquadratic point ($\phi = 0.5\pi$), where the empty circle denotes $S_z = 0$ and the filled one stands for $S_z = +1$ or -1.
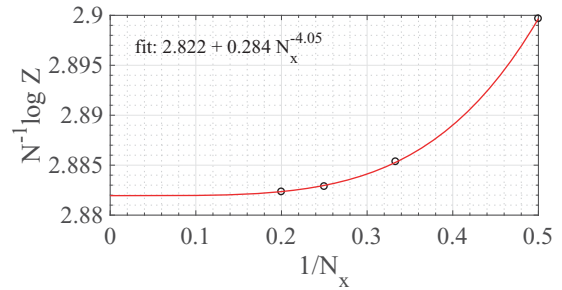

FIG. 6. The number of degenerate GS at $\phi = 0.5\pi$. The red solid line is the fitting curve. Here, the system is on the long cylinder with size $N = N_x N_y$ and $N_y \gg 1$.

the SU(3) symmetry and the FM state, and thus the FQ state can be mapped into each other by the SU(3) transformation. The cusp in the energy density and discontinuities in the derivative of energy density and order parameters at $\phi = 0.75\pi$ in Fig. 3 are in good agreement with the expectation and suggest the first-order phase transition. At this phase boundary, the FM state from SU and the FQ state from TR-symmetric SSU come to exactly the same energy density. This is the "state-switching" phase transition at the transition point with enhanced symmetry. Its classical example is the transition of U(1)-symmetric XXZ model from the easy-axis phase to the easy-plane phase at the SU(2)-symmetric point. The cusp and discontinuity in the energy and its derivative are also observed at the other boundary, $\phi = 0.5\pi$, suggesting the first-order transition here. However, we need to note that, in contrast to the BLBQ models defined on bipartite lattices, the present system does not possess the SU(3) symmetry at this phase boundary. Therefore, the mechanism of the transition must be somewhat different from the one at $\phi = -0.75\pi$. Nevertheless, this transition can still be located exactly. To see this, we note that there is a macroscopic GS degeneracy at $\phi = 0.5\pi$. More specifically, all product states containing no $(+1, -1)$ or $(0,0)$ nearest-neighbor pairs, where ± 1 or 0 are eigenvalues of S_z, are eigenstates of the Hamiltonian [63]. Thus, the transition point is located exactly at $\phi = 0.5\pi$ as the point where the entropy per spin becomes finite. A crude estimate of the lower bound for the GS entropy can be derived in the following way. Let us consider the following configurations: spins on the upward triangles form $\triangle$ (empty: $S_z = 0$, filled: $S_z = +1$ or -1) while ∇ or ∇ on the downward triangles. An example is shown in Fig. 5. The number of such configurations is simply $Z_0 = 2^{N_\triangle + N_\nabla}$ where $N_{\triangle(\nabla)}$ is the number of upward (downward) triangle plaquettes. The factor $2^{N_\triangle}$ comes from the fact that there are $N_\triangle$ clusters bounded by the 0 spins, whereas 2^{N_∇} from the choice between ∇ or ∇ for each downward triangle. Consequently, the entropy per spin is $S_{Z_0}/(6N) = \frac{1}{3} \log 2$, where N is the total number of unit-cell. In addition, we found that total number of all degenerate product states (Z) is equivalent to the number of muti-species dimer configurations with a particular constraint on the same lattice. Using a simple tensor

network, we have counted such dimer configurations (Fig. 6) and obtained a much better lower-bound for the entropy per spin $S_Z/(6N) = 0.4703$ (see Appendix for details).

Not only such simple product states but also some entangled states, e.g., the spin-singlet state, can be GS at $\phi = 0.5\pi$. By diagonalizing the Hamiltonian of 6- and 12-site systems, we find that a spin-singlet state is degenerate at the transition point, but becomes a unique GS with a finite BL interaction. On the other hand, our SU(2)-symmetric iPEPS at $\phi = 0.5\pi$ ansatz gives $E = 1.5026$, which deviates only 0.17% from the exact one $E = 1.5$. Therefore, we believe reasonably that the BL interaction lifts the macroscopic degeneracy such that the singlet state gains an advantage (lower energy) over the product states.

As for the transition around $\phi \simeq -0.23\pi$, after passing it from the FQ side to the AFM side, the order parameters (M, Q) and the derivative of energy density exhibit discontinuities around the transition (Fig. 3). Those evidences strongly suggest the first-order phase transition between the FQ and AFM phases.

VI. DISCUSSION

We have explored the GS phase diagram of the $S = 1$ BLBQ model on the star lattice with the state-of-art TN algorithms. In addition to FM, AFM, and FQ, gapped SL phases are identified by analyzing the local observables, various correlators, and transfer matrix. In the SL phase, the spin, dimer, quadrupole, and chirality correlators decay exponentially, and the correlation length converges to finite even at large bond dimensions of iPEPS ansatz. However, this phase has been characterized most clearly by the fact that it is represented by a PEPS with all the virtual legs of fixed parity: integer spins for intertriangle bonds and half-integer spins for the ones forming the triangles. While the state has something in common with the Haldane phase, in which all virtual bonds have odd parity, we are not aware of the cases where integer spins appear together with half-integer ones. A direct implication of this feature is that we may obtain different kinds of boundary excitations depending on the way we cut the system. Further investigation is desirable here. The nature of phase boundaries in the model are also investigated. We confirm the first-order phase transitions at $\phi = -0.75\pi$ and 0.5π by observing the phase coexistence and a finite correlation length, respectively. Particularly, the macroscopic degeneracy at $\phi = 0.5\pi$ is shown by counting the

partial number of degenerate GS by using the transfer matrix method (see the Appendix). The transition between FQ and AFM is also found to be the first order exhibiting the jumps in the order parameters and the derivative of energy. We believe that some of our work may be relevant for the star lattice antiferromagnet which has been synthesized with an iron(III) acetate hybrid material and its family [64]. We also expect to realize much of the discussed physics in optical lattices [65,66].

ACKNOWLEDGMENTS

APPENDIX: MACROSCOPIC DEGENERACY AT PURE BIQUADRATIC POINT

The biquadratic Hamiltonian with positive coupling reads

$$H_{BQ} = \sum_{\langle i,j \rangle} (\boldsymbol{S}_i \cdot \boldsymbol{S}_j)^2, \tag{A1}$$

where $\langle i,j \rangle$ denotes the nearest-neighbor sites. Each $(\boldsymbol{S}_i \cdot \boldsymbol{S}_j)^2$ operator has degenerate ground states, of which the total spin S_{ij}^{total} equals 1 and 2, with the eigenvalue $E = 1$. Therefore, configurations where all neighboring spins fuse to $S_{ij}^{\text{total}} = 1$ and 2 are the ground state of Eq. (A1). One can easily construct such states by avoiding the nearest-neighbor singlet pairs, i.e., $|+1, -1\rangle$ and $|0,0\rangle$, where $\pm1, 0$ are the S_z quantum number, in the whole lattice. An example on the star lattice is shown in Fig. 7(a). In one-dimensional chain, the total number of such configurations (Z) scales $Z \simeq 2^N$ and therefore the lower bound of the entropy density is $S/N = \log 2$ [67]. On the other hand, counting Z on the star lattice is not trivial because of the loops formed by the lattice sites. We first prove the macroscopic degeneracy and extract a crude estimate for the lower bound of the entropy density by counting exactly a part of Z. Then, the complete Z will be obtained numerically by employing a tensor network.
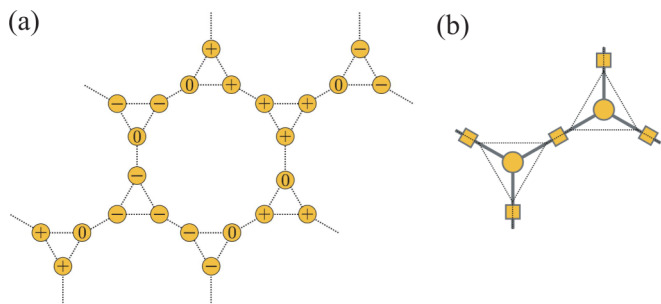

FIG. 7. (a) An exemplary ground-state configuration of the Hamiltonian in Eq. (A1), and (b) a proposed tensor network, made of plaquette and bond tensors, counting such configurations.
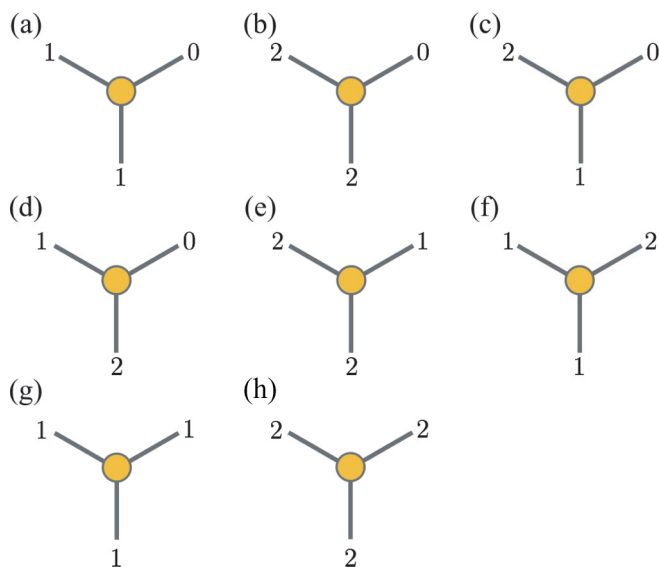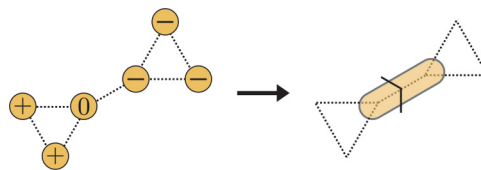

FIG. 8. Nonzero elements of the plaquette tensor P_{ijk} to count the configurations with only $S_z = 0, +1$ states.

One can map counting Z into a dimer packing problem with a particular constraint. The basic idea is the following. Let us regard the neighboring pair $|0, \pm1\rangle$ connecting two triangles as a directed (from 0 to ±1) dimer, e.g.,

Here, the direction is necessary to distinguish the configuration $|0, \pm1\rangle$ and $|\pm1, 0\rangle$. Therefore, we assign four species of dimers on every bond and then count the number of all dimer configurations allowing the hole with an equal weight. An additional constraint is that only a single outgoing dimer is permitted on every triangle plaquette at most. Now, one can count the total number of such dimer configurations by employing a simple tensor network composed of rank-three plaquette tensors (P_{ijk}) on the center of the triangle loop and bond matrices (B_{ij}) connecting P tensors as depicted in Fig. 7(b). For simplicity, let us first consider the configurations with only $S_z = 0, +1$ excluding the $S_z = -1$ state. Then, the bond dimension $D = 3$ is required, and each state on the leg can be defined as follows:

(1) $|0\rangle$: start point of dimer on the vertex,

(2) $|1\rangle$: end point of dimer on the vertex, and

(3) $|2\rangle$: hole on the vertex.

Because of the constraint allowing only a single outgoing dimer at most on each triangle plaquette, the configurations in Fig. 8 and their cyclic permutation partners are only nonzero elements of the tensor P_{ijk} while the bond matrix is

$$B = \begin{pmatrix} 0 & 1 & 0 \\ 1 & 0 & 0 \\ 0 & 0 & 1 \end{pmatrix}. \tag{A2}$$
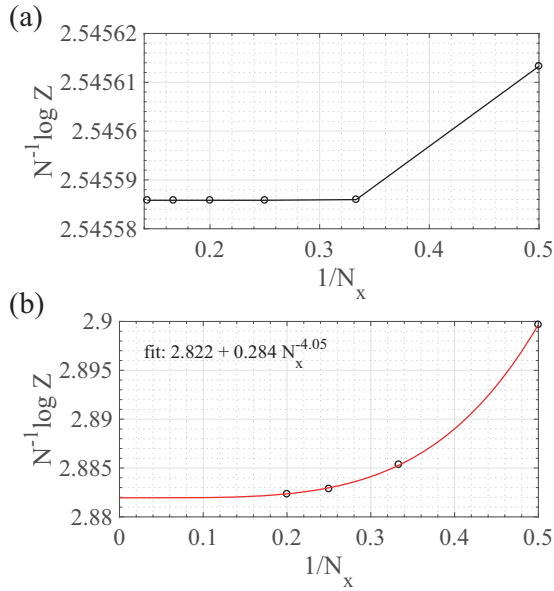
FIG. 9. The scaling of the number of GS configurations made of (a) $S_z = 0, +1$ and (b) $S_z = 0, \pm 1$, respectively.

We set the weight of each configuration in Fig. 8 to be 1, and then the contraction of the tensor network gives the total number of the ground states made of only $S_z = 0, +1$ states. Similarly, one may count the configurations even including $S_z = -1$ state by enlarging the bond dimension to $D = 5$.

Now, we contract two plaquette tensors and three bond tensors to have a translationally invariant tensor network on the square lattice. The efficient calculation of Z proceeds on a cylinder geometry with the periodic boundary condition imposed along the x direction of length N_x and open ends along the y direction of length N_y. By contracting the tensors along the x direction, one obtains the so-called row-to-row transfer matrix as schematically depicted below:
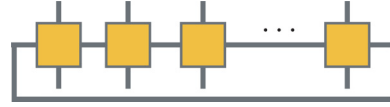
Assuming $N_y \gg 1$, the total number of configurations Z scales like $Z_{N_x} \simeq (\lambda_{N_x})^{N_y}$, where λ_{N_x} is the largest eigenvalue of the transfer matrix with a length N_x. Even though the transfer matrix is not Hermitian (or symmetric), the largest eigenvalue is unique and real by the Perron-Frobenius theorem [68]. In order to obtain the scaling behavior of Z in terms of the system size $N = N_x N_y$, we plot $N^{-1} \log Z_{N_x} = N_x^{-1} \log \lambda_{N_x}$. The result is presented in Fig. 9(a). As one can see, the entropy density with $N_x = 3$ is already very close to the one in the thermodynamic limit, which is $N^{-1} \log Z_{N_x=\infty} \simeq 2.54587$. We therefore conclude that the number of degenerate GS made of only $S_z = 0, +1$ states scales $Z \sim (e^{2.545587})^N = 12.75^N$.

By enlarging the bond dimension to $D = 5$, one can evaluate the degeneracy including $S_z = -1$ configurations. It is easy to find the nonzero elements of tensor, which is a straightforward extension from the elements in Fig. 8. The entropy density is shown in Fig. 9(b). Here, we extrapolate the data to obtain the one in the thermodynamic limit. Now, the number of degenerate states scales $Z \sim (e^{2.822})^N = 16.81^N$, and this can be regarded as the lower bound for the true entropy density of pure biquadratic model on the star lattice.

[1] J. G. Bednorz and K. A. Müller, Z. Phys. B **64**, 189 (1986).

[2] P. Anderson, Science **235**, 1196 (1987).

[3] X.-G. Wen, Phys. Rev. B **65**, 165113 (2002).

[4] A. Kitaev, Ann. Phys. **321**, 2 (2006).

[5] T.-H. Han, J. S. Helton, S. Chu, D. G. Nocera, J. A. Rodriguez-Rivera, C. Broholm, and Y. S. Lee, Nature (London) **492**, 406 (2012).

[6] X.-G. Wen, Phys. Rev. B **89**, 035147 (2014).

[7] F. D. M. Haldane, Phys. Rev. Lett. **50**, 1153 (1983).

[8] I. Affleck, T. Kennedy, E. H. Lieb, and H. Tasaki, Commun. Math. Phys. **115**, 477 (1988).

[9] Z.-C. Gu and X.-G. Wen, Phys. Rev. B **80**, 155131 (2009).

[10] F. Pollmann, E. Berg, A. M. Turner, and M. Oshikawa, Phys. Rev. B **85**, 075125 (2012).

[11] L. Balents, Nature (London) **464**, 199 (2010).

[12] Z. Hiroi, M. Hanawa, N. Kobayashi, M. Nohara, H. Takagi, Y. Kato, and M. Takigawa, J. Phys. Soc. Jpn. **70**, 3377 (2001).

[13] M. P. Shores, E. A. Nytko, B. M. Bartlett, and D. G. Nocera, J. Am. Chem. Soc **127**, 13462 (2005).

[14] H. Yoshida, N. Noguchi, Y. Matsushita, Y. Ishii, Y. Ihara, M. Oda, H. Okabe, S. Yamashita, Y. Nakazawa, A. Takata *et al.*, J. Phys. Soc. Jpn. **86**, 033704 (2017).

[15] Y. Shimizu, K. Miyagawa, K. Kanoda, M. Maesato, and G. Saito, Phys. Rev. Lett. **91**, 107001 (2003).

[16] M. Qazilbash, J. Hamlin, R. Baumbach, L. Zhang, D. J. Singh, M. Maple, and D. Basov, Nat. Phys. **5**, 647 (2009).

[17] Z. Yin, K. Haule, and G. Kotliar, Nat. Mater. **10**, 932 (2011).

[18] J. G. Cheng, G. Li, L. Balicas, J. S. Zhou, J. B. Goodenough, C. Xu, and H. D. Zhou, Phys. Rev. Lett. **107**, 197204 (2011).

[19] K. Harada and N. Kawashima, Phys. Rev. B **65**, 052403 (2002).

[20] K. Harada, N. Kawashima, and M. Troyer, J. Phys. Soc. Jpn. **76**, 013703 (2007).

[21] T. A. Tóth, A. M. Läuchli, F. Mila, and K. Penc, Phys. Rev. Lett. **108**, 029902(E) (2012).

[22] F. Wang, S. A. Kivelson, and D.-H. Lee, Nat. Phys. **11**, 959 (2015).

[23] C. Luo, T. Datta, and D.-X. Yao, Phys. Rev. B **93**, 235148 (2016).

[24] H. Lee and J. H. Han, Phys. Rev. B **94**, 115150 (2016).

[25] H. Lee, Y.-t. Oh, J. H. Han, and H. Katsura, Phys. Rev. B **95**, 060413 (2017).

[26] S.-S. Gong, W. Zhu, D. N. Sheng, and K. Yang, Phys. Rev. B **95**, 205132 (2017).

[27] I. Niesen and P. Corboz, Phys. Rev. B **95**, 180404 (2017).

[28] I. Niesen and P. Corboz, SciPost Phys. **3**, 030 (2017).

[29] W.-J. Hu, S.-S. Gong, H.-H. Lai, H. Hu, Q. Si, and A. H. Nevidomskyy, arXiv:1711.06523.

[30] Y.-W. Lee and M.-F. Yang, Phys. Rev. B **85**, 100402 (2012).

[31] H. H. Zhao, C. Xu, Q. N. Chen, Z. C. Wei, M. P. Qin, G. M. Zhang, and T. Xiang, Phys. Rev. B **85**, 134416 (2012).

[32] T. Liu, W. Li, A. Weichselbaum, J. von Delft, and G. Su, Phys. Rev. B **91**, 060403 (2015).

[33] A. Läuchli, F. Mila, and K. Penc, Phys. Rev. Lett. **97**, 087205 (2006).

[34] M. Serbyn, T. Senthil, and P. A. Lee, Phys. Rev. B **84**, 180403 (2011).

[35] A. Barabanov and V. Beresovsky, Phys. Lett. A **186**, 175 (1994).

[36] B. Canals and D. Garanin, Eur. Phys. J. B **26**, 439 (2002).

[37] P. Corboz, J. Jordan, and G. Vidal, Phys. Rev. B **82**, 245119 (2010).

[38] H. Yao and S. A. Kivelson, Phys. Rev. Lett. **99**, 247203 (2007).

[39] G. Kells, D. Mehta, J. K. Slingerland, and J. Vala, Phys. Rev. B **81**, 104429 (2010).

[40] B. Ware, J. H. Son, M. Cheng, R. V. Mishmash, J. Alicea, and B. Bauer, Phys. Rev. B **94**, 115127 (2016).

[41] B.-J. Yang, A. Paramekanti, and Y. B. Kim, Phys. Rev. B **81**, 134418 (2010).

[42] S.-J. Ran, W. Li, S.-S. Gong, A. Weichselbaum, J. von Delft, and G. Su, Phys. Rev. B **97**, 075146 (2018).

[43] G.-Y. Huang, S.-D. Liang, and D.-X. Yao, Eur. Phys. J. B **86**, 379 (2013).

[44] Y. Qi, Z.-C. Gu, and H. Yao, Phys. Rev. B **92**, 155105 (2015).

[45] R. Ors, Ann. Phys. **349**, 117 (2014).

[46] M. Levin and C. P. Nave, Phys. Rev. Lett. **99**, 120601 (2007).

[47] Z.-C. Gu, M. Levin, and X.-G. Wen, Phys. Rev. B **78**, 205116 (2008).

[48] S. Jiang and Y. Ran, Phys. Rev. B **92**, 104414 (2015).

[49] J.-W. Mei, J.-Y. Chen, H. He, and X.-G. Wen, Phys. Rev. B **95**, 235107 (2017).

[50] A. Schmitt, K.-H. Mütter, M. Karbach, Y. Yu, and G. Müller, Phys. Rev. B **58**, 5498 (1998).

[51] A. Läuchli, G. Schmid, and S. Trebst, Phys. Rev. B **74**, 144426 (2006).

[52] Z. Wang, W.-J. Hu, and A. H. Nevidomskyy, Phys. Rev. Lett. **116**, 247203 (2016).

[53] F. Verstraete, V. Murg, and J. I. Cirac, Adv. Phys. **57**, 143 (2008).

[54] H. C. Jiang, Z. Y. Weng, and T. Xiang, Phys. Rev. Lett. **101**, 090603 (2008).

[55] R. Baxter, J. Math. Phys. **9**, 650 (1968).

[56] T. Nishino and K. Okunishi, J. Phys. Soc. Jpn. **65**, 891 (1996).

[57] T. Nishino and K. Okunishi, J. Phys. Soc. Jpn. **67**, 3066 (1998).

[58] R. Orús and G. Vidal, Phys. Rev. B **80**, 094403 (2009).

[59] R. Orús, Phys. Rev. B **85**, 205117 (2012).

[60] S. Morita, mptensor: Parallel library for tensor network methods (2016–), https://github.com/smorita/mptensor.

[61] P. Corboz, S. R. White, G. Vidal, and M. Troyer, Phys. Rev. B **84**, 041108 (2011).

[62] P. Kim, H. Katsura, N. Trivedi, and J. H. Han, Phys. Rev. B **94**, 195110 (2016).

[63] M. Takahashi, *Thermodynamics of One-Dimensional Solvable Models* (Cambridge University Press, Cambridge, UK, 1999).

[64] Y.-Z. Zheng, M.-L. Tong, W. Xue, W.-X. Zhang, X.-M. Chen, F. Grandjean, and G. Long, Angew. Chem, Int. Ed. **46**, 6076 (2007).

[65] L.-M. Duan, E. Demler, and M. D. Lukin, Phys. Rev. Lett. **91**, 090402 (2003).

[66] J. Ruostekoski, Phys. Rev. Lett. **103**, 080406 (2009).

[67] K. Nomura and S. Takada, J. Phys. Soc. Jpn. **60**, 389 (1991).

[68] R. Horn and C. Johnson, *Matrix Analysis* (Cambridge University Press, Cambridge, UK, 1990).